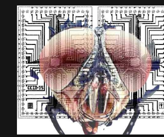

A CCD-based detector for CFHT's AO system

Olivier Lai, Kevin K.Y. Ho, Marc Baril, Jean-Charles Cuillandre, Chueh-Jen Lin, Tom Benedict, Jeff Ward, Derrick Salmon, Gerry Luppino, James Beletic, Reinhold Dorn, Pascal Puget, Barry Burke, Shiang-Yu Wang

Abstract Avalanche Photo-Diodes (APDs) have traditionally been used as detectors for wavefront sensing in curvature adaptive optics (AO) such as PUEO, the CFHT AO system. Passively quenched APDs are robust but have low QE (~40%), while actively quenched APDs can have much higher QE, but have been known to fail. Due to the cost of APDs, a CCD-based alternative is very attractive, especially in the case of a large number of sub-apertures. A technology project dubbed "FlyEyes" was conceived to evaluate and characterize the backside-illuminated CCID-35 detector as a suitable replacement for the APDs in the curvature wavefront sensor, thus providing a cost-effective upgrade path to converting PUEO to a higher-order system. Here we present the on-sky performance of FlyEyes as integrated in PUEO.

Integrating FlyEyes into the CFHT AO system - PUEO

The CFHT adaptive optics system, PUEO, has been in service since first light in 1996 and continues to see routine usage. PUEO is based on curvature wavefront sensing with a 19-element bimorph deformable mirror and 19 passively quenched APDs. Light from the wavefront is divided into 19 sub-pupils by a lenslet array and fed via optical fibers to the APDs. FlyEyes replaces the APDs with two CCID-35 detectors and an SDSU II controller. The optical fibers are removed from the APDs and rerouted to the CCID-35s. The diagram below shows a block diagram of PUEO and highlights where the CCID-35s integrates into PUEO.

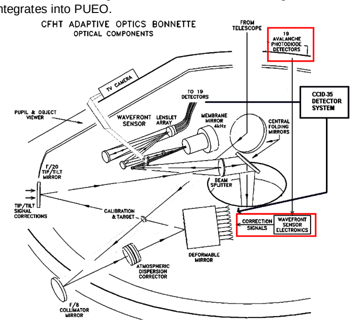

Figure 1: *(Above) The FlyEyes dewar built by Gerry Luppino. Note the pair of vacuum feedthroughs for the two CCID-35 sensors. Only one sensor is currently used in Flyeyes. (Left) Integration of FlyEyes in the PUEO instrument.*

A curvature sensing CCD: The CCID-35

The CCID-35 sensor was developed by the European Southern Observatory (ESO) in collaboration with the MIT-Lincoln Labs fabrication facility and was tailored specifically for use in curvature wavefront sensing. One of its unique design features are storage registers on either side of the imaging array that are used to integrate charge from the intra-focal and extra-focal images when curvature sensing. Charge may be transferred from the imaging area of each cell into one of three "storage" areas located on opposite sides of the imaging area. Having the storage registers eliminates the need to read out the images at each half cycle of the membrane mirror intra and extra-focal modulation (4 kHz in PUEO). The images are clocked out at 1 kHz, 500 Hz or 250Hz, depending on the intensity of the guide stars. Storage areas, SA and SB, store the charge for the half-cycle intra-focal and extra-focal images. The SC storage area is used to temporarily hold the charge as one half-cycle image is clocked out through the serial output register. Charge is binned into a super-pixel at the summing well before being output at the source follower amplifier.

The curvature sensing area of the CCID-35 consists of 10 columns containing 8 cells and a single 8 cell column used for tip/tilt sensing (not used in PUEO); see figure below. Each cell nominally consists of a 20 x 20 pixel imaging area (18 x 18 µm sized pixels) defined by the binning ratio. Each column of cells has its own serial output register and amplifier allowing rapid readout of the array with 8 output amplifiers. Readout noise should be less than 2 electrons for the CCID-35 to be considered a viable replacement for APDs, which have zero read noise.

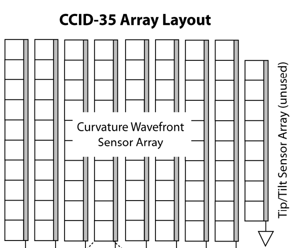

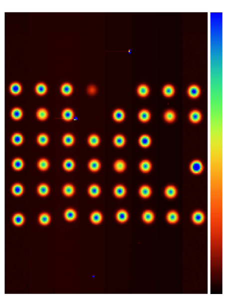

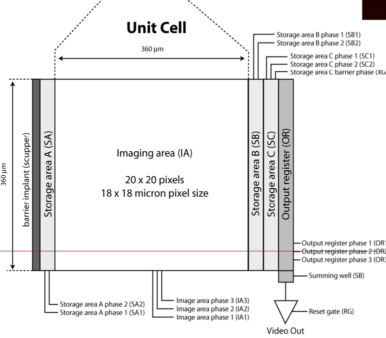

Figure 2: *(Top Right) Full frame image with no binning showing an afocal image of the fiber array located directly above the CCD. (Left) CCID-35 architecture showing the super-pixel unit cell (top) and the full array (below).*

Read noise

In photon counting detectors, the noise is integrated in the servo-loop and low frequencies are attenuated due to their improved SNR. Thus with APDs, the noise (*i.e.* the variance of the wavefront sensor signal) goes as N^{-1} with N the number of photons detected in a time interval, while when read noise is added in every frame, the noise goes as N^{-2} where the N photons have now been detected over many reads (*i.e.* the read noise accumulates in the loop). This is shown in Figure 3, which uses the formula for Shack-Hartmann wavefront sensors for the CCID-35, but still maintains the correct noise behavior. When the photon noise dominates, the WFS measurement variance for the APDs follows:

$$\sigma^2_{WFS} = \frac{7.2}{N_{photon} \cdot QE_{APD}} \ (\text{rad}^2)$$

where N_{photon} is the number of photons, and QE_{APD} is the APD quantum efficiency, 0.4 in this case. For the CCID-35, the WFS measurement variance is given by:

$$\sigma^2_{WFS} = \frac{\frac{1}{3}\pi^4 \cdot (\sigma_{read} \cdot n_{pixels})^2}{(N_{photon} \cdot QE_{CCD})^2} + \sigma^2_{\text{bandwidth}} \ (\text{rad}^2)$$

where the read noise per pixel σ_{read} is 1.8 e-, read over n_{pixels} (we assume 4), where N_{photon} is the number of photons, and QE_{CCD} is the CCID-35 quantum efficiency, assumed to be 0.9. The last term, $\sigma_{bandwidth}{}^2$ is the phase lag error and is required because increasing the integration time on the WFS can improve the SNR in terms of photons, at the expense of the temporal error determined by the Greenwood frequency and the loop correction frequency. In Figure 3, the Strehl attenuation is shown at 1 kHz with no phase lag error, at 500 Hz (twice the number of photons per sample) with a 0.2rad² phase lag error and at 250 Hz with a 0.8rad² phase lag error. This illustrates that on the bright end, a high sampling frequency is desirable to match the APD performance, despite the gain in QE, while at the faint end, the APD performance level can be emulated by lowering the sampling frequency. These simulations imply that by carefully adjusting the wavefront sensor frequency, the performance of PUEO should remain unaffected.

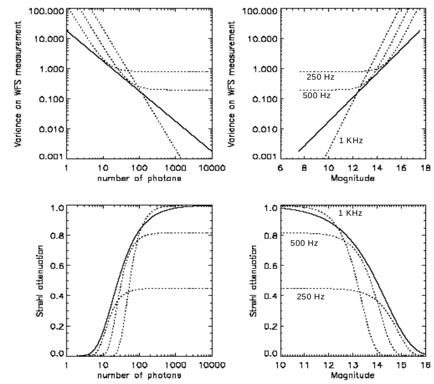

Figure 3: *Variance of WFS signal (top row) and equivalent Strehl attenuation (bottom row) for incident number of photons (left column) and equivalent Guide Star magnitude (right column) for APDs (full line) and CCID-35 (dotted line).*

Bright star performance

FlyEyes was tested on AOB on April 24th-26th 2007, February 25th-27th 2008 and a comparison run with the APDs took place on December 17th-18th 2007. Figure 4 plots the delivered Strehl ratio as a function of r_0 at the wavelength of observation and shows that the bright star performance is unaffected when using FlyEyes. The black crosses show the original 1996 integration data, which consisted of more than 300 observations of stars at all wavelengths in varying conditions. The red diamonds show the dynamic Strehl ratio measured on images obtained in April 2007 as a function of the r_0 estimated from the wavefront sensor data; these lie at the expected location on the curve.

Also shown is a picture of Saturn obtained on April 27th at 9:00UTC while guiding on Dione, which was magnitude 10.2 at the time. Images were obtained in J, H and K bands to produce the true color image shown in Figure 4 (right).

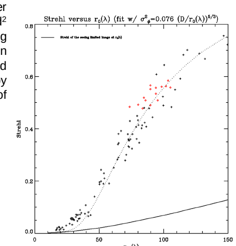

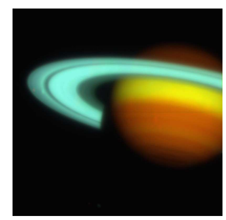

Figure 4: *(Left) Bright guide star performance, showing the delivered Strehl ratio as a function of $r_0(\lambda)$; 1996 PUEO integration data, black crosses, April 2007 data using FlyEyes, red diamonds. (Right) Saturn, observed on April 27th 2007 at UT 9:00. Wavefront sensing with FlyEyes was performed on Dione.*

Faint star performance

The comparison with APDs turned out to be more difficult than anticipated due to varying seeing and τ_0 conditions. Nonetheless, by recording and correcting for the r_0 estimated by the wavefront sensor data, we were able to confirm that the performance was not noticeably degraded by using FlyEyes instead of the APDs. The modal control of PUEO works by estimating the input phase power spectrum from the measured residual power spectrum from the WFS and a model of its well-known and characterized transfer function. Using this information it is possible to optimize the loop gain in closed loop automatically. We were unable to implement a full modal control for FlyEyes as this would have required modeling/measuring the transfer functions for the different sampling frequencies and loop gains under controlled conditions. Instead we ran our tests with either modal control enabled, or with zonal control enabled while setting the gain manually. This made the testing cumbersome, but a sufficient number of data points were collected to see trends emerging (Figure 5). The left column in Figure 5 shows the number of detected photons translated into magnitudes as a function of the guide star magnitude. Some spread can be expected due to varying photometric conditions and spectral type. At 1 kHz, the effect of read noise begins to appear at magnitude15.4. The middle column shows the raw Strehl ratio, as measured on the imaging detector as a function of the guide star magnitude. The scatter is understandable as there is no accounting for either the actual detected number of photons or r_0 at the time of the observations. The top and bottom of panels represent the modal and zonal gain control respectively. The spread is such that it is hard to infer any quantitative assessment of performance. Qualitatively, it appears that above magnitude 11, the performance is improved by lowering the sampling frequency. The right column shows the final result, accounting for the static Strehl ratio, the number of detected photons and r_0. The small black diamonds are the dynamic Strehl at 1 kHz (*i.e.* corrected only for static aberrations). The red crosses show the same data corrected for r_0, and can thus be regarded as a Strehl attenuation. One will note that scatter in the Strehl attenuation at the lower sampling frequencies is lower. A best-fit model to the data is shown in the blue curves (see paper for an explanation of the dashed curves). There is a fair agreement especially for the 250Hz data at the faint end, although the spread in the data, probably due to varying conditions of the atmosphere, prevented us from finding a clean cross-over of performance for various sampling frequencies as expected from the model (*i.e.* Figure 3).

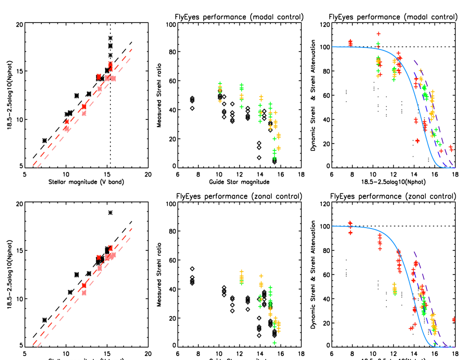

Figure 5: *Flyeyes performance as a function of guide star magnitude. (Left) photometry. (Center) Recorded Strehl. (Right) Strehl attenuation. Black, green and yellow symbols in center and right are for 1 kHz, 500 Hz and 250 Hz sampling, respectively. Top row is with PUEO modal control, lower row is with zonal control at various gains.*

Conclusions **The FlyEyes experiment has successfully demonstrated the use of CCDs as an alternative to APDs in PUEO. The CCID-35 has better quantum efficiency than the passively quenched APDs used in PUEO, however it has a finite read noise of ~2e-. FlyEyes was integrated with PUEO and successful sky operation was achieved on bright stars with V<10. On fainter stars, 10 < V < 16, FlyEyes performed as well as APDs, although varying atmospheric conditions prevented us from obtaining repeatable performance as a function of magnitude. Operationally, it would be desirable to determine the optimal sampling frequency as a function of guide star magnitude. The demand for PUEO is constant but low, so there is no immediate plan to use FlyEyes as a replacement for the APDs as it would require additional integration and characterization effort. However, should the CFHT user community decide that an upgrade of PUEO is necessary, the perfect detector is ready and waiting…**